# Computation of Human-Sperm Local Flagellar Instantaneous Velocity

Dan Sidney Díaz-Guerrero[1], Fernando Montoya[1], Haydee Olínca Hernández[2], Paul Hernández-Herrera[3], Alberto Darszon[4], and Gabriel Corkidi[1(✉)]

[1] Laboratorio de Imágenes y Visión por Computadora, Departamento de Ingeniería Celular y Biocatálisis, Instituto de Biotecnología, Universidad Nacional Autónoma de México, Cuernavaca, Morelos, Mexico
gabriel.corkidi@ibt.unam.mx

[2] Posgrado en Ciencia e Ingeniería de la Computación, Universidad Nacional Autónoma de México, Cuernavaca, Morelos, Mexico

[3] Laboratorio Nacional de Microscopía Avanzada, Universidad Nacional Autónoma de México, Cuernavaca, Morelos, Mexico

[4] Departamento de Genética del Desarrollo y Fisiología Molecular, Instituto de Biotecnología, Universidad Nacional Autónoma de México, Cuernavaca, Morelos, Mexico

**Abstract.** The instantaneous velocity generated by human-sperm flagellum is key for the fundamental description and understanding of flagellar movement and sperm motility. Furthermore, since the flagellar movement is intrinsically three-dimensional, only with 3D dynamic data of the flagellar trajectory it is feasible to compute the instantaneous velocity of flagellar point elements. It was only recently that real flagellar 3D+t motility data were available, which is indispensable for the calculation of instantaneous velocity. In this work we present the first results of flagellar instantaneous velocity obtained from $3D+t$ data of human sperm by means of a Fourier fitting method. One descriptor and its distribution over the sperm sample are presented to compare the experimental conditions (induced to capacitate, and not induced to capacitate as control) related to the fertilization process. While the descriptor distributions are evidently distinct across both experimental conditions, a statistical analysis confirmed this difference supporting the visual perception and importance of the finding.

**Keywords:** Instantaneous velocity · Fourier transform · Fourier series · Vector resultant · Human sperm · 3D microscopy

## 1 Introduction

The study of sperm motility has been mainly based on the bidimensional (2D) head trajectory over time [2,14–19,21,23,26]. This approach has made possible important advances in basic research (see [9] and references therein) and in the health sciences [20]. Nonetheless, this framework is clearly incomplete as sperm


J. de J. A. Flores Cuautle et al. (Eds.): CNIB 2023, IFMBE Proceedings 96, pp. 59–66, 2024.
https://doi.org/10.1007/978-3-031-46933-6_7

swim in three dimensions (3D) in certain regions of the female reproductive tract. A comprehensive understanding of the sperm dynamics needs to incorporate the third spatial dimension and the flagellum. This approach was technologically impaired until about 20 years ago [7]. Recently there have been numerous and important developments (see [5,6,8,10,11,25]) that include the flagellar beating in the sperm motility analysis of sperm flagellar beating [4,6,13].

More recently [13], an experimental setup and a methodological framework were developed to obtain dynamical 3D human whole-sperm data (3D+t). This opened a myriad of possible research lines regarding flagellar motility. However, this significant achievement came with big challenges in the form of enormous quantities of images and numerical data.

In this work, the 3D + t data set consists of 60744 data files (from 147 sperm), each containing the x, y, z coordinates of the segmented flagellum [12]. Each cell belongs to one of two conditions: not induced to capacitate (NoCap, 60 cells) and induced to capacitate (Cap, 87 cells). Using these data, a Fourier series was constructed and used to compute the instantaneous velocity for the mid-flagellar point for each one of the 147 sperm cells in the dataset. The Fourier series of the component functions allowed us to compute instantaneous velocities, and opening other scientific venues.

## 2 Methodology

The $x, y, z$ coordinates of a sperm at a given time will be called a flagellar curve, thus the entire trajectory of a given sperm will consist of $T$ flagellar curves. Due to the experimental setup there are 90 flagellar curves per second [13]. For instance, if there are 270 flagellar curves for a given sperm, then the time recorded is three seconds.

To compute the instantaneous velocity of each point of the flagellum, first let's use the position vector notation

$$\{\mathbf{r}_{i,t}\}_{i=0}^{n-1} = \{\mathbf{r}_{0,t}, \mathbf{r}_{1,t}, \ldots, \mathbf{r}_{n-1,t}\} \tag{1}$$

where $\mathbf{r}_{i,t} = (x_i(t), y_i(t), z_i(t))$ is the $i$-th flagellar point at time $t$. The flagellar point with index $i = 0$ represents the head-flagellum junction and the last flagellar point index $i = n - 1$ represents the tail of the flagellum. For instance, take a given point of the flagellum, let's say the ninth point at time five, then it is denoted by $\mathbf{r}_{9,5} = (x_9(5), y_9(5), z_9(5))$. So, the instantaneous velocity at the point $\mathbf{r}_{i,t}$ is its time derivative, this is denoted by $\dot{\mathbf{r}}_{i,t}$. Although there are several options to compute discrete derivatives, in general they all have numerical instabilities. Considering this, the ideal option is to have the mathematical expression of the function describing the experimental points over time, a difficult solution to achieve. However, there are feasible options: series expansions of mathematical functions. Therefore, it is necessary to obtain an accurate curve fitting of $\mathbf{r}_{i,t}$ over time. Let's call this curve a time-point curve, that is the set $\{\mathbf{r}_{i,t}\}$ for $t \in \{1, 2, \ldots, T\}$ (abbreviated as $\{\mathbf{r}_{i,t}\}_{t=1}^{T}$) at a fixed flagellar position $i$ over the flagellum, see Fig. 1.

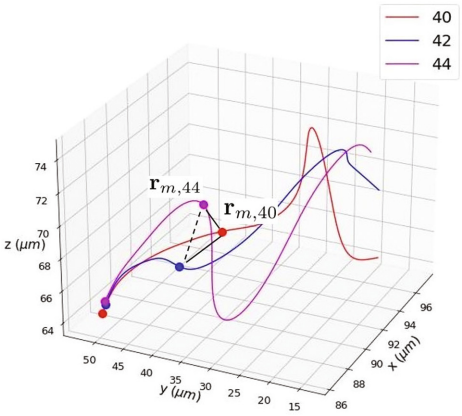


**Fig. 1.** Flagellar curves, corresponding to times 0.44, 0.47, and 0.49 s (or indices 40, 42, 44). The points in the lower left corner indicate the head of the flagellum, meanwhile the points in the middle are precisely their middle points. Therefore, fixing the flagellar point to value $m$ and considering all the registered times one gets the time-point curve indicated by joining the middle points with lines.

The Taylor series are frequently used to expand a mathematical function. In the Taylor series each term involves a derivative of the objective function, so the mathematical expression of the function must be known *a priori*. Nevertheless, there is another well known series more suited to the case of time-point curves that is the Fourier series. One of the advantages of these series is that they do not use the derivative of the objective function. The Fourier series require the Fourier transform and their associated frequencies, as shown next in Eq. 2.

$$g(t) = \frac{1}{n} \sum_{k=0}^{n-1} \phi(k) \exp(2\pi j \varepsilon(k) t) \tag{2}$$

where $j$ is the imaginary unit ($j^2 = -1$), $\exp(t)$ is the exponential function, and $\phi(k)$ is the $k$-th point of the Fourier transform, and $\varepsilon(k)$ is its frequency. Given the Fourier series, its time derivative is straight-forward

$$\frac{d}{dt} g(t) = \frac{2\pi j}{n} \sum_{k=0}^{n-1} \phi(k) \varepsilon(k) \exp(2\pi j \varepsilon(k) t). \tag{3}$$

Hence, by numerically computing the Fourier transform and its frequencies a time-point curve is modeled by its Fourier series of the form (2) with the corresponding Fourier transform and frequencies, computed numerically with *python-numpy-fft* package.

## 3 Results

The Fourier-models of the function components $(x_i(t), y_i(t), z_i(t))$ over time for the time-point curve $\{\mathbf{r}_{i,t}\}_{t=1}^{T}$ were obtained and used to compute the instantaneous velocity. Thus, $\mathbf{r}_{i,t} = (g_x(t), g_y(t), g_z(t))$ for each $t \in \{1, 2, \ldots, T\}$. Here $g_x(t), g_y(t), g_z(t)$ are obtained by applying Eq. 2 to $x_i(t), y_i(t), z_i(t)$, respectively. In Fig. 2 a comparison of the model with the experimental $3D + t$ points is illustrated.

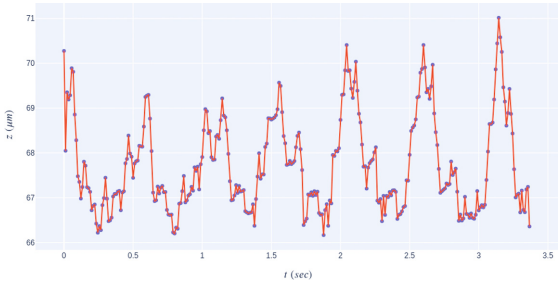


**Fig. 2.** Fourier model. The experimental data points of the $z_0(t)$ function component are plotted in blue, their corresponding Fourier series is plotted in red with lines for visual clarity.

Given the excellent fitting of the experimental points by the Fourier model, we used the velocity (Eq. 3) on all three $x_i(t), y_i(t), z_i(t)$ function components and for all flagellar points. The latter process produces the set of velocities $\{\dot{\mathbf{r}}_{i,t}\}_{i=0}^{n-1}$ for $t \in \{1, 2, \ldots, T\}$. As this set consists of all the velocities for every point for each sperm in the dataset, we choose the middle flagellar point to apply a statistical analysis of the velocities. Even with the restriction to one point, there are 147 sperm and several times for each one of them. Therefore, we considered one descriptor based on the norm of the velocity vectors: the norm-resultant velocity.

The norm-resultant velocity (Eq. 4) is an integrative measure, as it is the norm of the vector sum of all the velocities. In Fig. 3 the violin plots of the norm-resultant velocity for each sperm conditions are shown. The resultant velocity vector is the vector sum of the velocities of the middle flagellar point over all available times.

$$\|\dot{\mathbf{r}}_{res}\| = \left\| \sum_{t=1}^{T} \dot{\mathbf{r}}_{m,t} \right\|. \tag{4}$$

The norm-resultant velocity distributions for both conditions are visually distinguishable. In the NoCap condition, the distribution is more uniformly dispersed over its range. Meanwhile, in the Cap condition its distribution is localized over its boxplot.

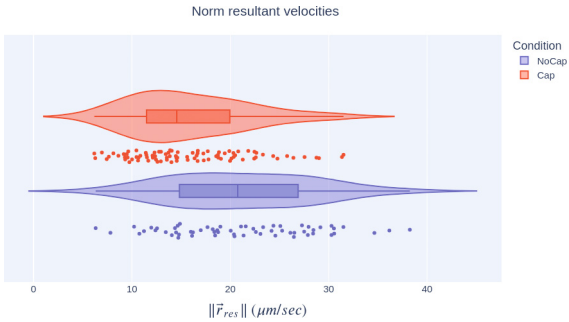


**Fig. 3.** Norm-resultant velocity distributions. This is a single descriptor for each sperm cell defined as the euclidean norm of the resultant velocity vector for the middle flagellar point. In this figure the norm-resultant velocity is used to compare both experimental conditions: spermatozoa not induced to capacitate (NoCap), and spermatozoa induced to capacitate (Cap). It is visually clear that those cells induced to capacitate have a more localized norm-resultant velocity distribution.

In the norm-resultant distribution it seems that there are more sperm, for the Cap condition, with values less than 10 $\mu$m/s (see Fig. 3). This suggests that induction to capacitate changes the distribution of the velocity vectors of the middle flagellar point. This change is such that more sperms have norm-resultant values lower than most of the sperms for the NoCap condition.

A statistical analysis of significance was applied to the Norm Resultant Velocities (NRVs). First, a Shapiro-Wilk normality test was conducted, yielding a p-value of 0.002. This value implies that the data does not follow a normal distribution. Second, a Wilcoxon signed-rank test was performed, resulting in a p-value of 0.02. This p-value allows us to reject the null hypothesis that the NRVs for both the NoCap and Cap conditions come from the same distribution.

In summary, based on the obtained results, it can be concluded that the Norm Resultant Velocities (NRVs) do not follow a normal distribution and that NoCap and Cap conditions have significant different distributions.

## 4 Discussion and Conclusions

The knowledge of the instant velocity for every single flagellar point is of great value due to the possible venues of research that it opens, such as the analysis of the local forces and their relation with hydrodynamics. Furthermore, with the results presented in this work there are differences in the distributions of the considered descriptor for conditions NoCap and Cap. The existence of statistical differences is of crucial importance in this context. This significance stems from the fact that, according to the literature (e.g., [3]), only a relatively small percentage, ranging from 10 to 20%, of cells under the Cap condition attain hyperactivation. Moreover, the diversity in local dynamical properties could obscure hyperactivation features. However, among those cells with a norm

resultant velocity lower than 10 μm/s it is possible that local hyperactivation characteristics may be exhibited.

A key element in the presented analysis is the local character of the instantaneous velocity. In fact, this locality is the reason why this descriptor was selected to give global information about each cell. But this doesn't imply that a local analysis is not possible or desirable. On the contrary, it indicates that local analysis for both experimental conditions could be very relevant as there are features in the Cap condition absent in the NoCap sample.

However, a local analysis is as interesting as is challenging due to the size of the set of velocity vectors, and its diversity (magnitudes and directions). In this sense, previous findings [4,21] showed that a hyperactivated sperm could display motility features belonging to both NoCap and Cap conditions. Thus, a local analysis demands not only to know if a sperm was or wasn't induced to capacitate, but the identification of the flagellar curves (times) that have distinctive features too. In this line of thought it would be ideal to have a labeled set of hyperactivated sperms (those sperm cells induced to capacitate that truly reach capacitation), this would enable a target-oriented analysis with the main aim of locally characterizing the hyperactivated motility features.

Recently other features of the flagellar beating have been studied: the second harmonics of human flagellar sperm beat [24], the flagellar energetics of beating patterns in mouse sperm [22], and the change of flagellar beating forces before and after capacitation in human sperm [1]. These will be complemented and may be improved by our results because, although in this work only the flagellar midpoint was considered, the methodology described above can be directly applied to any point in the dataset. In contrast the methodology described in [1] is limited to the tip-point of the sperm tail.

In conclusion, we implemented a Fourier fitting method and used it to compute the instantaneous velocity of a mid-flagellar point. Based on this set of instantaneous velocity vectors we proposed a descriptor which showed differences between the two experimental conditions under consideration. Moreover, the obtained set of instantaneous velocity has a wide potential of describing the local details of flagellar dynamics. This local level of accuracy in the flagellar movement is only limited by the experimental setup from which the dataset was obtained.

Meanwhile, the immediate research question that can, and will be, explored are those concerning with the characterization of the distinctive flagellar forms that are empirically identified as signatures of hyperactivated sperm cells. Also, the flagellar movement in different viscosity conditions will be analyzed under the hypothesis that due to high viscosity the average curvature over the flagellum should decrease.

**Notes and Acknowledgments.** This work involved human subjects in its research. Approval of all ethical and experimental procedures and protocols was done by the Bioethics Committee from Instituto de Biotecnología, UNAM. Signed written informed consent forms were signed by all healthy donors. This work was supported in part by Dirección General de Asuntos del Personal Académico, Universidad Nacional

Autónoma de México under the Grants IN204922 and IN105222. The work of Paul Hernández-Herrera was supported by the Chan Zuckerberg Initiative DAF under the Grant 2020-225643. The work of D. S. Díaz-Guerrero and H. O. Hernández was supported by a Posdoctoral fellowship and Ph.D. scholarship respectively, from CONACYT-Mexico.

## References

1. Battistella, A., Andolfi, L., Stebel, M., Ciubotaru, C., Lazzarino, M.: Investigation on the change of spermatozoa flagellar beating forces before and after capacitation. Biomater. Adv. **145**, 213242 (2023)
2. Brokaw, C.J.: Microtubule siliding in swimming sperm flagella: direct and indirect measurements on sea urchin and tunicate spermatozoa. J. Cell Biol. **114**(6), 1201–1215 (1991)
3. Cohen-Dayag, A., Tur-Kaspa, I., Dor, J., Maschiach, S., Eisenbach, M.: Sperm capacitation in humans is transient and correlates with chemotactic responsiveness to follicular factors. Proc. Natl. Acad. Sci. U.S.A. **92**, 11039–11043 (1995)
4. Corkidi, G., Hernández-Herrera, P., Montoya, F., Gadêlha, H., Darszon, A.: Long-term segmentation-free assessment of head-flagellum movement and intracellular calcium in swimming human sperm. J. Cell Sci.**134**(3), jcs250654 (2021)
5. Corkidi, G., et al.: Are there intracellular Ca2+ oscillations correlated with flagellar beating in human sperm? A three vs. two-dimensional analysis. Mol. Hum. Reprod. **23**(9), 583–593 (2017)
6. Corkidi, G., Taboada, B., Wood, C.D., Guerrero, A., Darszon, A.: Tracking sperm in three-dimensions. Biochem. Biophys. Res. Commun. **373**(1), 125–129 (2008)
7. Crenshaw, H.C.: Analysis of three-dimensional trajectories of organisms: estimates of velocity, curvature and torsion from positional information. J. Exp. Biol. **203**, 961–982 (2000)
8. Gadêlha, H., Hernandez-Herrera, P., Montoya, F., Darszon, A., Corkidi, G.: Human sperm uses asymmetric and anisotropic flagellar controls to regulate swimming symmetry and cell steering. Sci. Adv. **6**(31) (2020)
9. Gaffney, E.A., Ishimoto, K., Walker, B.J.: Modelling motility: the mathematics of spermatozoa. Front. Cell Dev. Biol. **9**, 71082 (2021)
10. Guerrero, A., Carneiro, J., Pimentel, A., Wood, C.D., Corkidi, G., Darszon, A.: Strategies for locating the female gamete: the importance of measuring sperm trajectories in three spatial dimensions. Mol. Hum. Reprod. **17**(8), 511–523 (2011)
11. Hernandez-Herrera, P., Montoya, F., Rendón, J.M., Darszon, A., Corkidi, G.: Sperm Flagellum Center-Line Tracing in Fluorescence 3D+t Low SNR Stacks Using an Iterative Minimal Path Method. In: Karray, F., Campilho, A., Cheriet, F. (eds.) ICIAR 2017. LNCS, vol. 10317, pp. 437–445. Springer, Cham (2017). https://doi.org/10.1007/978-3-319-59876-5_48
12. Hernández-Aviña, H.O., et al.: Feature-based 3D+t descriptors of hyperactivated human sperm beat patterns. bioRxiv, 4 (2023)
13. Hernández-Herrera, P., Montoya, F., Rendón-Mancha, J.M., Darszon, A., Corkidi, G.: 3-D+t human sperm flagellum tracing in low snr fluorescence images. IEEE Trans. Med. Imaging **37**, 2236–2247 (2018)
14. Katz, D.F., Cherr, G.N., Lambert, H.: The evolution of hamster sperm motility during capacitation and interaction with the ovum vestments in vitro. Gamete Res. **14**, 333–346 (1986)

15. Katz, D.F., Davis, R.O.: Automatic analysis of human sperm motion. J. Androl. **8**, 170–181 (1987)
16. Katz, D.F., Diel, L., Overstreet, J.W.: Differences in the movement of morphologically normal and abnormal human seminal spermatozoa. Biol. Reprod. **26**(4), 566–570 (1982)
17. Mortimer, D., Kossakowski, J., Mortimer, S.T., Fussell, S.: Prediction of fertilizing ability by sperm kinematics. J. Assist Reprod. Genet. **14**(5), 525 (1997)
18. Mortimer, D., Pandya, I.J., Sawers, R.S.: Relationship between human sperm motility characteristics and sperm penetration into human cervical mucus in vitro. J. Reprod. Fertil. **78**(1), 93–102 (1986)
19. Mortimer, D., Mortimer, S.T.: Influence of system parameter settings on human sperm motility analysis using cellsoft. Hum. Reprod. **3**(5), 621–625 (1988)
20. Mortimer, S.T.: Casa-practical aspects. J. Androl. **21**, 515–524 (2000)
21. Mortimer, S.T., Swan, M.A.: Variable kinematics of capacitating human spermatozoa. Hum. Reprod. **10**(12), 3178–3182 (1995)
22. Nandagiri, A., et al.: Flagellar energetics from high-resolution imaging of beating patterns in tethered mouse sperm. eLife **10** (2021)
23. Owen, D.H., Katz, D.F.: Sampling factors influencing accuracy of sperm kinematic analysis. J. Androl. **14**(3), 210–221 (1993)
24. Saggiorato, G., Alvarez, L., Jikeli, J.F., Kaupp, U.B., Gompper, G., Elgeti, J.: Human sperm steer with second harmonics of the flagellar beat. Nat. Commun. **8**(1), 1415 (2017)
25. Sánchez-Cárdenas, C., et al.: Intracellular Ca2+ threshold reversibly switches flagellar beat off and on. Biol. Reprod. **99**(5), 1010–1021 (2018)
26. Suarez, S.S., Katz, D.F., Overstreet, J.W.: Movement characteristics and Overstreet. and acrosomal status of rabbit spermatozoa recovered at site and time of fertilization. Biol. Reprod. **29**(5), 1277–1287 (1983)